Detecting Fibroblast Activation Proteins in Lymphoma Using ^{68}Ga-FAPI PET/CT

Xiao Jin*[1], Maomao Wei*[1], Shuailiang Wang*[1], Guochang Wang*[1], Yumei Lai[2], Yunfei Shi[2], Yan Zhang[1], Zhi Yang[1], and Xuejuan Wang[1]

[1]*Key Laboratory of Carcinogenesis and Translational Research (Ministry of Education) and NMPA Key Laboratory for Research and Evaluation of Radiopharmaceuticals (National Medical Products Administration), Department of Nuclear Medicine, Peking University Cancer Hospital and Institute, Beijing, China; and* [2]*Department of Pathology, Peking University Cancer Hospital and Institute, Beijing, China*

Cancer-associated fibroblasts that overexpress fibroblast activation protein (FAP) are enriched in many epithelial carcinomas and in hematologic neoplasms. PET/CT with radiolabeled FAP inhibitor (FAPI) is a new diagnostic tool for visualizing the tumor stroma. This prospective study aimed to profile FAPs in different subtypes of lymphomas and explore the potential utility of ^{68}Ga-FAPI PET/CT in lymphomas. **Methods:** In this prospective study, we recruited 73 lymphoma patients who underwent ^{68}Ga-FAPI PET/CT and recorded and measured semiquantitative parameters and ratios of their scan results. FAPI expression was assessed by immunochemistry in samples obtained from 22 of the lymphoma patients. **Results:** We evaluated 11 patients with Hodgkin lymphoma and 62 with non-Hodgkin lymphoma (NHL). Significantly elevated FAP uptake was observed in Hodgkin lymphoma lesions, correlating with the intensity of FAP immunostaining (score, 3+). A positive association was found between the corresponding clinical classification of NHL and the ^{68}Ga-FAPI uptake activity of the lesion. Aggressive NHL lesions, with moderate to strong FAP immunostaining (score, 2+ to 3+), exhibited intense to moderate ^{68}Ga-FAPI uptake. Indolent NHL lesions showed weak FAP staining and mild to moderate ^{68}Ga-FAPI uptake. No statistically significant correlation emerged between the sum of the product of the diameters and the corresponding SUV_{max} ($P = 0.424$). The tumor-to-liver ratios were 6.26 ± 4.17 in indolent NHL and more than 9 in other subtypes. **Conclusion:** ^{68}Ga-FAPI imaging can be used to detect FAP expression in lymphoma lesions and may be an alternate method for characterizing lymphoma profiles.

Key Words: ^{68}Ga-FAPI PET; lymphoma; cancer-associated fibroblasts; fibroblast activation protein; tumor stroma

J Nucl Med 2022; 63:212–217
DOI: 10.2967/jnumed.121.262134

Lymphomas are a heterogeneous group of malignancies arising from lymphocytes and typically involve lymphoid organs. They account for approximately 3.5% of new malignant cases worldwide, with B-cell lymphomas (BCLs) and Hodgkin lymphoma (HL) accounting for 80% and 10% of all lymphoma cases, respectively. Lymphoma pathogenesis is well understood, and there is increasing focus on nonmalignant cells residing in the tumor, primarily immune and stromal cells, which constitute the so-called tumor microenvironment (*1*).

Recent studies have suggested that the outcome of patients with lymphoma is entwined with the remarkable heterogeneity of both the malignant clone and the cellular/extracellular microenvironment and unveiled fibroblasts in the microenvironment that might exhibit both a protumorigenic and an antitumorigenic phenotype (*2*,*3*). A stromal gene signature representing fibroblasts has been shown to correlate with poor survival in carcinomas, including breast, ovarian, pancreatic, and colorectal cancer. Paradoxically, a closely related gene signature has been associated with good survival in BCLs (*4*,*5*). This contradictory result has generated lots of interest and effort in elucidating fibroblast-mediated effects. Even though these studies indicated that stromal signatures of BCLs could predict survival, they were clinically restrained by the lack of robust and reproducible biomarkers (*6*,*7*). Additionally, to support histopathologic and genic evidence, the tumor stroma needs to be visualized and monitored, and imaging is an essential aspect of the diagnostic workup.

Nonhematopoietic (CD45-negative) tumor stroma in lymphoid tissues comprise cells of mesenchymal origin and vascular endothelial cells (*8*). Cancer-associated fibroblasts (CAFs) belong to the CD45-negative–reprogrammed myelofibroblastic network and play a crucial role in the development and progression of solid tumors (*9*). CAFs and activated fibroblasts selectively overexpress a growth factor, fibroblast activation protein (FAP). Molecular PET/CT imaging with radiolabeled FAP inhibitor (FAPI) has been evaluated in various diseases but not in lymphoma (*10*,*11*). Recently, we incidentally found a mild ^{68}Ga-FAPI uptake in a primary gastric diffuse large BCL (DLBCL) lesion. Thus, we hypothesize that CAFs in lymphoma can be imaged using ^{68}Ga-FAPI PET/CT (*12*).

The aim of this prospective study was to identify FAPs with ^{68}Ga-FAPI-04 PET/CT in different subtypes of lymphomas (especially T-cell lymphoma), quantify ^{68}Ga-FAPI-04 accumulations in nodal and extranodal lesions, and explore the potential utility of ^{68}Ga-FAPI-04 PET/CT in lymphomas.

MATERIALS AND METHODS

Patients

This prospective study was approved by the Institutional Review Board of our hospital (approval 2019KT95) and registered with ClinicalTrials.gov (NCT04367948). Written informed consent was obtained from the patients for receiving ^{68}Ga-FAPI PET/CT examinations and

Received Feb. 15, 2021; revision accepted Apr. 21, 2021.
For correspondence or reprints, contact Xuejuan Wang (xuejuan_wang@hotmail.com).
*Contributed equally to this work.
Published online May 28, 2021.

the publication of their anonymous data accompanying the imaging results. Study enrollment was performed from December 2019 to August 2020. The patient inclusion criteria were a pathologic diagnosis of lymphoma, an age of 18–75 y, expected survival of at least 12 wk, and a minimum of 1 target lesion with ^{68}Ga-FAPI uptake. The exclusion criteria were severe liver or kidney dysfunction, pregnancy or lactation, inability of the patient to lie on the scanner bed for less than 0.5 h, and inability or unwillingness of the patient or legal representative to provide written informed consent. The final study cohort comprised 73 patients with lymphoma. The study flowchart of patient enrollment is presented as Supplemental Figure 1 (supplemental materials are available at http://jnm.snmjournals.org).

Radiopharmaceuticals

Synthesis and radiolabeling of ^{68}Ga-FAPI-04 were performed as previously described. Briefly, ^{68}Ga was chelated after pH adjustment with sodium acetate. Then, a reaction mixture of 25 μg (28.6 nmol) of FAPI-04 and 1.7 GBq of ^{68}Ga solution was heated to 100°C for 10 min. Next, the reaction solution was diluted to 5 mL and passed through a preconditioned Sep-Pak C18 Plus Light Cartridge (Waters), and the cartridge was eluted with 0.5 mL of 75% ethanol to obtain the final product. Quality control of the radiosynthesis was performed by ultraviolet and radio-high-performance liquid chromatography, and the radiochemical purity was more than 95%. The ^{68}Ga-FAPI injections were filtered through a 0.22-μm Millex-LG filter (EMD Millipore) before clinical use.

PET/CT Imaging

The radiopharmaceutical was administrated intravenously at a dose of 1.8–2.2 MBq/kg. At approximately 60 ± 10 min after injection, a torso acquisition (n = 52) of 6–8 bed positions (1 min/bed position) commenced using a hybrid system (Philips Gemini TF PET/CT scanner) that covered from the base of the skull to the upper thigh. Non–contrast-enhanced CT was performed using 100-mA modulation, 120 kV, and a slice thickness of 3 mm for attenuation correction and anatomic localization purposes. The dedicated head acquisition was separately performed at 1 bed position (8–10 min/bed position). Acquisitions from the top of the skull to the upper thigh or the tip of the toes were performed on the remaining 21 patients. The emission data were corrected for random, scatter, and decay. The data were reconstructed using the ordered-subset expectation maximum algorithm to obtain coronal, sagittal, and cross-sectional PET and PET/CT images. The total scan time was approximately 19 min. The patients were asked to self-report any abnormalities at 30 min after the PET/CT scans.

Image Interpretation

Three experienced nuclear physicians were assigned to independently interpret each patient's PET images with knowledge of the clinicopathologic data on a Philips EBW workstation. The presence and sites of lymphoma involvement and the intensity of the ^{68}Ga-FAPI uptake in the lesions were recorded for each PET scan. Increased radioactivity compared with the background uptake was considered positive and was measured and calculated via the region-of-interest technique. Any discordant results were resolved by consensus. Up to 6 of the largest or highest SUV_{max} lymphoma lesions were identified from different body regions for each PET/CT scan. The product of the diameters was calculated by multiplying the longest diameter by the shortest diameter for each lesion. Then, the products of the diameters were added to assess the sum of products of the diameters (SPD), which was representative of the patient's overall disease burden. The nonspecific background in the liver was quantified with a circular 2-cm-diameter sphere, and the tumor-to-liver ratio was calculated.

Immunohistochemistry

FAP expression in lymphoma lesions was determined using post-surgical histology samples from 7 patients and biopsy samples from 15 patients via immunohistochemistry performed as per a previous report. Before immunohistochemistry staining, the tissue sections were stained with hematoxylin and eosin and reviewed by *2* experienced pathologists. FAP was detected using a rabbit monoclonal antibody against FAP (BM5121; Boster). Briefly, formalin-fixed, paraffin-embedded blocks were cut into 4-μm-thick sections, deparaffinized in xylene, and rehydrated. Antigen was retrieved using ethylenediaminetetraacetic acid (pH 8.0; Santa Cruz Biotechnology) in a pressure cooker for 3 min. Then, the sections were incubated in 3% H_2O_2 solution for 10 min at room temperature to block endogenous peroxidase activity. Immunohistochemistry was performed with anti-FAP antibody at a dilution of 1:400 for 12 h at 4°C. Subsequently,

TABLE 1
Clinical Features of 73 Patients with Lymphoma

Parameters	No. of patients
Sex	
Male	37 (50.68%)
Female	36 (49.32%)
Age	
>60 y	26 (35.62%)
≤60 y	47 (64.38%)
Treatment type	
Initial assessment	48 (65.75%)
Progressed	17 (23.29%)
Relapsed	8 (10.96%)
Lesion distribution	
Nodal only	15 (20.55%)
Extranodal, primary	19 (26.03%)
Both	39 (53.42%)
Histologic subtype	
HL	11 (15.07%)
NHL	62 (84.93%)
DLBCL	34 (46.57%)
ENKTCL	5 (6.85%)
AITL	4 (5.48%)
PMBL	2 (2.74%)
BL	1(1.37%)
MCL	1 (1.37%)
B-LBL	1 (1.37%)
C-ALCL	1 (1.37%)
$CD8^+$ AECTCL	1 (1.37%)
FL	9 (12.33%)
MALT lymphoma	2 (2.74%)
CLL/SLL	1 (1.37%)

ENKTCL = extranodal natural killer/T-cell lymphoma; AITL = angioimmunoblastic T-cell lymphoma; PMBL = primary mediastinal large BCL; BL = Burkitt lymphoma; MCL = mantle cell lymphoma; B-LBL - B lymphoblastic leukemia/lymphoma; C-ALCL = primary cutaneous anaplastic large-cell lymphoma; $CD8^+$ AECTCL = cutaneous CD8-positive aggressive epidermotropic cytotoxic T-cell lymphoma; FL= follicular lymphoma; CLL/SLL = chronic lymphocytic leukemia/small lymphocytic lymphoma.

TABLE 2
SUV_{max} of Nodal and Extranodal Lymphoma Lesions

			Nodal			Extranodal			
Lymphoma group	Histology	Patients (*n*)	Average	Median	Range	Average	Median	Range	*P*
Initial	HL	6	11.78 ± 4.03	11.8	7.3–18.1	7.20 ± 2.55	7.2	5.4–9.0	0.18
	DLBCL	22	8.52 ± 4.57	8.4	2.3–20.2	10.14 ± 4.33	10.9	3.7–17.1	0.08
	ENKTCL	3	5.40 ± 3.14	6.8	1.8–7.6	7.93 ± 1.12	8.2	6.7–8.9	0.29
	AITL	3	6.57 ± 2.40	6	4.5–9.2	2.4	2.4	NA	NA
	PMBL	2	18.40 ± 6.01	20.2	11.7–23.3	NA	NA	NA	NA
	BL	1	NA	NA	NA	19.1	19.1	NA	NA
	B-LBL	1	2.3	2.3	NA	6.5	6.5	NA	NA
	MCL	1	NA	NA	NA	5.1	5.1	NA	NA
	FL	7	5.60 ± 2.71	5.4	1.7–9.8	7.95 ± 3.68	8.05	4.2–11.5	0.47
	MALT lymphoma	1	NA	NA	NA	1.8	1.8	NA	NA
	CLL/SLL	1	5.9	5.9	NA	4.5	4.5	NA	NA
	Total	48	8.35 ± 4.87	7.6	1.7–23.3	8.92 ± 6.08	8.2	1.8–19.1	0.11
Progressed	HL	3	9.63 ± 4.05	8.6	6.2–14.1	5.90 ± 5.44	3.7	1.9–12.1	0.29
	DLBCL	8	7.87 ± 1.89	8.7	4.3–9.7	9.40 ± 6.40	6.8	2.8–21.0	0.36
	CD8+ AECTCL	1	NA	NA	NA	8.4	8.4	NA	NA
	ENKTCL	1	NA	NA	NA	7.5	7.5	NA	NA
	AITL	1	4.9	4.9	NA	NA	NA	NA	NA
	MALT	1	4.9	4.9	NA	5.6	5.6	NA	NA
	FL	2	5.5	5.5	4.3–6.7	12.3	12.3	NA	NA
	Total	17	7.49 ± 2.68	7.05	4.3–14.1	8.38 ± 5.23	7.15	1.9–21.0	0.60
Relapsed	HL	2	7.45 ± 3.75	7.45	4.8–10.1	6.75 ± 2.62	6.75	4.9–8.6	NA
	DLBCL	4	5.67 ± 5.23	3.7	1.7–11.6	7.63 ± 3.68	6.65	4.4–12.8	0.96
	ENKTCL	1	NA	NA	NA	8.7	8.7	NA	NA
	C-ALCL	1	NA	NA	NA	5.2	5.2	NA	NA
	Total	8	6.38 ± 4.26	4.8	1.7–11.6	7.24 ± 2.80	6.65	4.4–12.8	0.95

ENKTCL = extranodal natural killer/T-cell lymphoma; AITL = angioimmunoblastic T-cell lymphoma; NA = not applicable; PMBL = primary mediastinal large BCL; BL = Burkitt lymphoma; B-LBL = B lymphoblastic leukemia/lymphoma; MCL = mantle cell lymphoma; FL = follicular lymphoma; CLL/SLL = chronic lymphocytic leukemia/small lymphocytic lymphoma; $CD8^+$ AECTCL = cutaneous CD8-positive aggressive epidermotropic cytotoxic T-cell lymphoma; C-ALCL = primary cutaneous anaplastic large-cell lymphoma.

antirabbit IgG-horseradish peroxidase-linked secondary antibody was applied for 30 min at 37°C. Then, the sections were developed with 3,3′-diaminobenzidine tetrahydrochloride. Mayer hematoxylin was applied for 5 min as a counterstain. Photographs of representative fields were taken using an N-Achroplan objective (Zeiss). The FAP expression was assessed visually and quantitatively. Stromal cell staining was scored as 0 (absence of FAP immunostaining), 1+ (weak FAP staining in <10% of stromal cells), 2+ (positive FAP immunostaining in 10%–50% of stromal cells), and 3+ (moderate to strong FAP immunostaining in >50% of stromal cells) (*13*).

Statistical Analysis

All statistical analyses were conducted using SPSS software (version 20.0; IBM Corp.). SUVs were presented as the mean ± SD. The Kolmogorov–Smirnov test was used to determine whether the data were normally distributed. Comparisons between the average SUV_{max} were made using the *t* test or Mann–Whitney *U* test. The correlation between SUV_{max} and histologic subtypes was evaluated by the Pearson correlation coefficient. A *P* value of less than 0.05 was considered statistically significant.

RESULTS

Patient Characteristics

We enrolled 73 patients (36 women and 37 men; age, 51.6 ± 14.2 y; range, 21–74 y) in our study. Of them, 48 had newly diagnosed lymphoma, 17 had progressive disease, and 8 had relapses. Non-Hodgkin lymphoma (NHL; *n* = 62, 84.93%) was the most prevalent pathologic subtype, including DLBCL (*n* = 34, 46.57%), follicular lymphoma (*n* = 9, 12.33%), extranodal natural killer/T-cell lymphoma (*n* = 5, 6.85%), angioimmunoblastic T-cell lymphoma (*n* = 4, 5.48%), primary mediastinal large BCL (*n* = 2, 2.74%), and mucosa-associated lymphoid tissue (MALT) lymphoma (*n* = 2, 2.74%). The other enrolled subtypes had 1 case each. Fifteen cases (20.55%) involved only lymph nodes, and 19 (26.02%) were primary extranodal lymphomas (Table 1).

TABLE 3
Size and SPD of Lymphoma Lesions

		Node size (cm)			SPD		
Histologic subtype	Patients (*n*)	Median	Average	Range	Median	Average	Range
HL	11	10.07	14.14 ± 13.22	2.53–47.23	27.13	41.44 ± 32.10	8.28–95.00
DLBCL	34	7.88	9.93 ± 12.12	3.55–58.83	35.43	43.51 ± 47.78	11.99–229.49
ENKTCL	5	2.53	2.29 ± 0.81	1.39–2.95	10.55	14.12 ± 7.86	7.09–24.47
AITL	4	4.60	4.58 ± 1.69	2.56–6.58	26.55	25.76 ± 18.36	2.56–47.36
PMBL	2	7.99	9.06 ± 4.99	3.55–19.35	39.61	38.02 ± 17.45	15.49–67.02
BL	1	NA	NA	NA	18.18	18.18	18.18
MCL	1	NA	NA	NA	15.89	15.89	15.89
B-LBL	1	2.71	2.71	2.71	43.03	43.03	43.03
C-ALCL	1	NA	NA	NA	2.10	2.10	2.10
$CD8^+$ AECTCL	1	NA	NA	NA	8.96	8.96	8.96
FL	9	5.40	8.23 ± 8.49	2.78–39.99	31.35	31.89 ± 18.40	5.56–70.88
MALT lymphoma	2	2.17	2.17	2.17	3.22	3.22 ± 1.57	2.11–4.33
CLL/SLL	1	8.84	8.84	8.84	32.6	32.6	32.6

ENKTCL = extranodal natural killer/T-cell lymphoma; AITL = angioimmunoblastic T-cell lymphoma; PMBL = primary mediastinal large BCL; BL = Burkitt lymphoma; NA = not applicable; MCL = mantle cell lymphoma; B-LBL = B lymphoblastic leukemia/lymphoma; C-ALCL = primary cutaneous anaplastic large-cell lymphoma; $CD8^+$ AECTCL = cutaneous CD8-positive aggressive epidermotropic cytotoxic T-cell lymphoma; FL = follicular lymphoma; CLL/SLL = chronic lymphocytic leukemia/small lymphocytic lymphoma.

Quantifying ^{68}Ga-FAPI-04 Uptake in Lymphoma Lesions

The ^{68}Ga-FAPI-04 PET/CT scans were visually positive for detecting lymphoma in 72 of 73 (98.6%) patients because of the low background, except a patient with primary gastric MALT lymphoma. The average SUV_{max}, median SUV_{max}, and SUV_{max} range of the lymphoma lesions were 9.46 ± 4.61, 8.9, and 1.7–23.3, respectively. The average SUV_{max} of the initial assessment, progressed, and relapsed groups was 9.74 ± 4.88, 9.37 ± 5.03, and 8.35 ± 2.57, respectively ($P = 0.769$). The overall SUV_{max} (7.98 ± 4.39 vs. 8.49 ± 4.45), median SUV_{max} (7.3 vs. 7.5) and SUV_{max} range (1.7–23.0 vs. 1.8–21.0) of ^{68}Ga-FAPI in nodal and extranodal lesions did not differ ($P > 0.05$). Similar results were found in various histologic subtypes ($P > 0.05$) (Table 2).

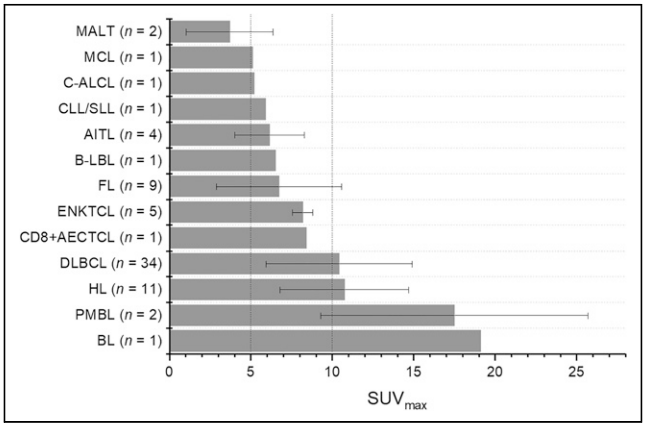

FIGURE 1. Average SUV_{max} of ^{68}Ga-FAPI PET/CT in various histologic subtypes. MCL = mantle cell lymphoma; C-ALCL = primary cutaneous anaplastic large-cell lymphoma; CLL/SLL = chronic lymphocytic leukemia/small lymphocytic lymphoma; AITL = angioimmunoblastic T-cell lymphoma; B-LBL = B lymphoblastic leukemia/lymphoma; FL = follicular lymphoma; ENKTCL = extranodal natural killer/T-cell lymphoma; CD8+AECTCL = cutaneous CD8-positive aggressive epidermotropic cytotoxic T-cell lymphoma; PMBL = primary mediastinal large BCL; BL = Burkitt lymphoma.

The lymph node sizes and SPDs in different histologic subtypes are shown in Table 3. The mean SPD, median SPD, and SPD range of lymphoma lesions were 34.22 ± 34.46, 25.54, and 2.10–229.49, respectively. No statistically significant correlation emerged between the SPD and corresponding SUV_{max} ($r = 0.107$, $P = 0.424$).

All tumor entities exhibited a high interindividual and intralesional SUV variation (Fig. 1). The highest average SUV_{max} (>10) was found in primary mediastinal large BCL, Burkitt lymphoma, HL, and DLBCL. The lowest ^{68}Ga-FAPI intensity (average $SUV_{max} < 5$) was observed in MALT lymphoma. Other subtypes showed moderate ^{68}Ga-FAPI uptake (average SUV_{max}, 5–10). No statistically significant difference was found between the SUV_{max} of HL (10.74 ± 3.95) and NHL (9.23 ± 4.71) ($P = 0.323$). SUV_{max} was significantly higher for BCLs (9.97 ± 4.68) than for T-cell lymphomas (7.19 ± 1.73) ($P = 0.002$). Figure 2 exhibits various extranodal sites in the enrolled patients.

According to the clinical classification for NHL, the average SUV_{max} of ^{68}Ga-FAPI in aggressive ($n = 50$) lymphoma was significantly higher than in indolent ($n = 12$) lesions (9.97 ± 4.68 vs. 6.16 ± 3.57; $P = 0.008$). Correlation analysis revealed a moderate correlation between the clinical classification and SUV_{max} ($r = 0.338$, $P = 0.007$). Because of the low background activity (average SUV_{mean} of liver, 1.11 ± 0.36), the tumor-to-liver ratios were 9.89 ± 6.08, 10.03 ± 5.12, and 6.26 ± 4.17 in HL, aggressive NHL, and indolent NHL, respectively.

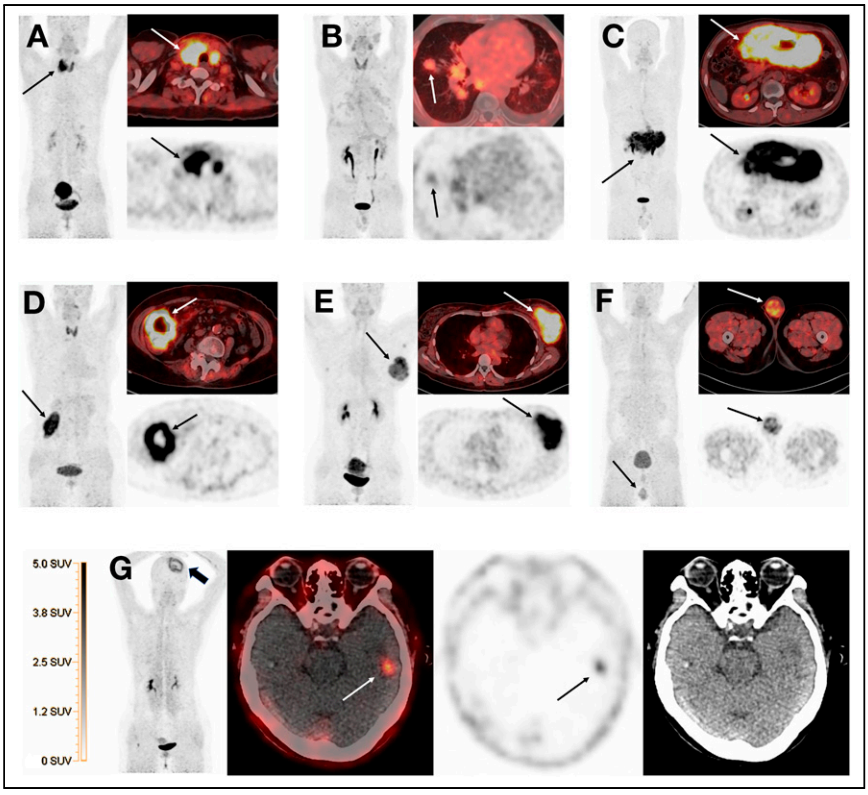

FIGURE 2. Maximum-intensity projections, axial ^{68}Ga-FAPI PET, and fused images (left, top right, and bottom right, respectively, in each panel) of various extranodal sites in enrolled patients. (A) Primary thyroid Burkitt lymphoma (arrows). (B) HL with lung involvement (arrows). (C) Primary gastric DLBCL (arrows). (D) Ileum DLBCL (arrows). (E) Left breast DLBCL (arrows). (F) Left testicle DLBCL (arrows). (G) Left temporal lobe DLBCL lesion (thin arrows) after left frontal lymphoma resection (thick arrow).

Immunohistochemistry

To further characterize FAP as a target structure within lymphoma, we performed FAP immunohistochemistry in 22 of the included cases. There were 4 patients with HL and 18 patients with NHL (9 DLBCL, 2 extranodal natural killer/T-cell lymphoma, 1 angioimmunoblastic T-cell lymphoma, 1 mantle cell lymphoma, 3 follicular lymphoma, 1 MALT lymphoma, and 1 chronic lymphocytic leukemia/small lymphocytic lymphoma).

The pathologic examinations showed intense FAP expression (score, 3+) in all HL lesions (4/4). For NHL, 7 of 12 aggressive lesions scored 3+ for FAP immunostaining, 4 of 5 indolent lesions showed weak FAP expression (score, 1+), and 5 of 9 DLBCL lesions overexpressed FAP (score, 3+). Weak FAP expression (score, 1+) was detected in MALT lymphoma lesions. Surprisingly, chronic lymphocytic leukemia/small lymphocytic lymphoma lesions showed moderate FAP expression (score, 2+). Furthermore, lesions with intense FAP expression exhibited an higher SUV_{max} than lesions that scored 1+, and a statistically significant correlation was unmasked between the SUV_{max} of lymphoma lesions and FAP expression ($b = 0.551$, $P < 0.001$). Figure 3 shows representative examples of the FAP immunostaining results.

DISCUSSION

The most crucial contribution of our study is the first visualization of FAPs in malignant lymphoid tumors, particularly in T-cell lymphomas. Moreover, we quantified the accumulation of ^{68}Ga-FAPI ligand in different subtypes of lymphoma lesions.

Fibroblastic reticular cells are specialized myofibroblasts that create the lymph node skeleton with its conduit system (*14*). Malignant cells recruit and reeducate their surrounding cells to establish a tumor-supportive milieu that also affects the biology and function of fibroblastic reticular cells. Once reprogrammed to CAFs, they can induce extracellular matrix remodeling (*15*). There is increasing evidence that CAFs can potentially regulate tumor progression in hematologic neoplasms. Lenz et al. (*3*) and Haro et al. (*4*) reported that the stromal-1 gene signature was associated with good survival in patients with DLBCL and several other BCLs. Paradoxically, Bankov et al. (*7*) and Aronovich et al. (*16*) demonstrated that fibroblasts in classic HL and mycosis fungoides promoted tumor cell migration and drug resistance. These conflicting results indicate that there is still much to learn about the biologic and clinical significance of CAFs in different lymphoma subtypes. Thus, a new strategy is necessary to depict tumor–stroma interaction in lymphoma that does not involve visualization using morphologic or metabolic imaging.

Biologically, ^{68}Ga-FAPI PET/CT is an excellent imaging modality to visualize FAP expression in the tumor stroma (*10*,*17*). Most false-positive results occur in wound healing and inflammatory or fibrosis conditions caused by the activation, proliferation,

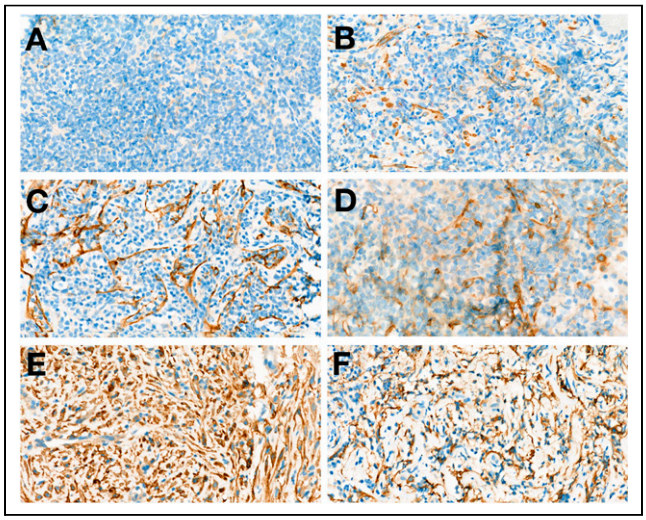

FIGURE 3. FAP immunohistochemistry of 6 exemplary cases of lymphoma. (A and B) Follicular lymphoma (A) and MALT with mild stromal FAP expression and FAP-negative neoplastic cells (B). (C and D) Chronic lymphocytic leukemia/small lymphocytic lymphoma (C) and DLBCL with moderate stromal FAP expression (D). (E and F) DLBCL (E) and HL with intense stromal FAP expression (F).

and accumulation of fibroblasts (*11*). Although clinical evaluations of ^{68}Ga/^{18}F-FAPI PET have been performed in a spectrum of cancers, there are none involving lymphomas. In our study, 72 lymphoma patients referred for ^{68}Ga-FAPI PET imaging showed FAPI-positive lesions in most subtypes of lymphoma, including both BCLs and T-cell lymphomas, except a patient with MALT lymphoma.

Since the origin, number, and distribution of FAP-expressing CAFs, as well as the number of FAP molecules per cell, may differ in tumors, we expect variations in tumor uptake and in the intratumoral tracer distribution. HL, especially the nodular sclerosing subtype of classic HL, is characterized by fibroblast proliferation in the tumor microenvironment, leading to fibrotic bands surrounding the lymphoma infiltrate. In our study, we found intense FAP immunostaining and significantly elevated FAPI uptake in HL lesions. Regarding NHL, there was a positive association between the clinical classification of NHL and the ^{68}Ga-FAPI uptake activity of the lesion in PET/CT imaging. Aggressive NHL, especially DLBCL, exhibited intermediate to intense ^{68}Ga-FAPI uptake and showed moderate to strong FAP immunostaining. These results were consistent with Haro and Orsulic's findings, who reported a high proportion of CAFs in B-cell lymphomas via a stromal gene signature analysis (*4*). Less common aggressive NHL subtypes, such as mantle cell lymphoma, B-lymphoblastic leukemia/lymphoma, primary cutaneous anaplastic large-cell lymphoma, and angioimmunoblastic T-cell lymphoma, with moderate FAP expression (score, 2+), exhibited moderate ^{68}Ga-FAPI avidities. Surprisingly, we noted that follicular lymphoma, which showed the lowest desmoplastic reaction by histopathology, had intermediate ^{68}Ga-FAPI uptake (SUV_{max}, 6.69 ± 3.85). MALT lymphoma, which showed weak FAP staining, exhibited mild ^{68}Ga-FAPI uptake, as expected. However, we did not expect that T-cell lymphoma would accumulate less ^{68}Ga-FAPI, even though the lesions expressed moderate to intense FAP expression.

Because of the very low background activity for ^{68}Ga-FAPI, especially in the brain, liver, and peritoneal cavity, the high tumor-to-background ratios resulted in high contrast ratios for lymphoma lesions, particularly in the brain, liver, and oropharynx. These may be advantageous for the detection of cerebral, hepatic, or oropharyngeal involvement. As previous studies have reported, we also easily identified a DLBCL lesion in the left temporal lobe in our study.

Because of the limitations of this report, such as a heterogeneous patient collective and a low case number for some subtypes, further studies are necessary. Furthermore, because of the lack of follow-up, analysis of the long-term prognosis regarding disease-free and overall survival is currently unfeasible. Therefore, larger prospective clinical studies are needed for further evaluation.

CONCLUSION

Our study results showed that ^{68}Ga-FAPI PET/CT is an extremely useful technique for profiling FAP expression status in lymphoma lesions. HL and aggressive NHL may possess more CAFs in tumor stroma than does indolent disease.

DISCLOSURE

This work was financially supported by the National Natural Science Foundation of China (no. 82071957), special funding from the Beijing Hospitals Authority Clinical Medicine Development (code XMLX202120), and Capital's Funds for Health Improvement and Research (no. 2018-2-1024). No other potential conflict of interest relevant to this article was reported.

KEY POINTS

QUESTION: Can ^{68}Ga-FAPI PET/CT detect FAPs in lymphoma?

PERTINENT FINDINGS: In this prospective study of 73 lymphoma patients, we found that ^{68}Ga-FAPI PET/CT could be used to profile FAP expression status in lymphoma lesions. Furthermore, HL and aggressive NHL may possess more FAPs in tumor stroma than does indolent disease.

IMPLICATIONS FOR PATIENT CARE: ^{68}Ga-FAPI imaging may be an alternate method for characterizing lymphoma profiles.

REFERENCES

1. Höpken UE, Rehm A. Targeting the tumor microenvironment of leukemia and lymphoma. *Trends Cancer.* 2019;5:351–364.
2. Augsten M. Cancer-associated fibroblasts as another polarized cell type of the tumor microenvironment. *Front Oncol.* 2014;4:62.
3. Lenz G, Wright G, Dave SS, et al. Stromal gene signatures in large-B-cell lymphomas. *N Engl J Med.* 2008;359:2313–2323.
4. Haro M, Orsulic S. A paradoxical correlation of cancer-associated fibroblasts with survival outcomes in B-cell lymphomas and carcinomas. *Front Cell Dev Biol.* 2018;6:98.
5. Ciavarella S, Vegliante MC, Fabbri M, et al. Dissection of DLBCL microenvironment provides a gene expression-based predictor of survival applicable to formalin-fixed paraffin-embedded tissue. *Ann Oncol.* 2018;29:2363–2370.
6. Staiger AM, Duppel J, Dengler MA, et al. An analysis of the role of follicular lymphoma-associated fibroblasts to promote tumor cell viability following drug-induced apoptosis. *Leuk Lymphoma.* 2017;58:1922–1930.
7. Bankov K, Döring C, Ustaszewski A, et al. Fibroblasts in nodular sclerosing classical Hodgkin lymphoma are defined by a specific phenotype and protect tumor cells from brentuximab-vedotin induced injury. *Cancers (Basel).* 2019;11:1687.
8. Roozendaal R, Mebius RE. Stromal cell-immune cell interactions. *Annu Rev Immunol.* 2011;29:23–43
9. Kalluri R. The biology and function of fibroblasts in cancer. *Nat Rev Cancer.* 2016;16:582–598.
10. Kratochwil C, Flechsig P, Lindner T, et al. ^{68}Ga-FAPI PET/CT: tracer uptake in 28 different kinds of cancer. *J Nucl Med.* 2019;60:801–805.
11. Altmann A, Haberkorn U, Siveke J. The latest developments in imaging of fibroblast activation protein. *J Nucl Med.* 2021;62:160–167.
12. Wang G, Jin X, Zhu H, et al. ^{68}Ga-NOTA-FAPI-04 PET/CT in a patient with primary gastric diffuse large B cell lymphoma: comparisons with [^{18}F] FDG PET/CT. *Eur J Nucl Med Mol Imaging.* 2021;48:647–648.
13. Serfling S, Zhi Y, Schirbel A, et al. Improved cancer detection in Waldeyer's tonsillar ring by ^{68}Ga-FAPI PET/CT imaging. *Eur J Nucl Med Mol Imaging.* 2021;48:1178–1187.
14. Roozendaal R, Mebius RE, Kraal G. The conduit system of the lymph node. *Int Immunol.* 2008;20:1483–1487.
15. Öhlund D, Elyada E, Tuveson D. Fibroblast heterogeneity in the cancer wound. *J Exp Med.* 2014;211:1503–1523.
16. Aronovich A, Moyal L, Gorovitz B, et al. Cancer-associated fibroblasts in mycosis fungoides promote tumor cell migration and drug resistance through CXCL12/CXCR4. *J Invest Dermatol.* 2021;141:619–627.e2.
17. Lindner T, Loktev A, Altmann A, et al. Development of quinoline-based theranostic ligands for the targeting of fibroblast activation protein. *J Nucl Med.* 2018;59:1415–1422